

OPTIMIZED SCHWARZ METHODS FOR THE COUPLING OF CYLINDRICAL GEOMETRIES ALONG THE AXIAL DIRECTION

GIACOMO GIGANTE¹ AND CHRISTIAN VERGARA^{2,*}

Abstract. In this work, we focus on the Optimized Schwarz Method for circular flat interfaces and geometric heterogeneous coupling arising when cylindrical geometries are coupled along the axial direction. In the first case, we provide a convergence analysis for the diffusion-reaction problem and jumping coefficients and we apply the general optimization procedure developed in Gigante and Vergara (*Numer. Math.* **131** (2015) 369–404). In the numerical simulations, we discuss how to choose the range of frequencies in the optimization and the influence of the Finite Element and projection errors on the convergence. In the second case, we consider the coupling between a three-dimensional and a one-dimensional diffusion-reaction problem and we develop a new optimization procedure. The numerical results highlight the suitability of the theoretical findings.

Mathematics Subject Classification. 65N12, 65B99.

Received February 28, 2017. Accepted May 25, 2018.

1. INTRODUCTION

The Optimized Schwarz Method (OSM) is a well established Domain Decomposition method based on looking for efficient parameters in Robin-like interface conditions [25, 30]. This method has been considered for many problems, such as the advection-reaction-diffusion problem [16, 26], the Helmholtz equation [17, 31], the shallow-water equations [35], the Maxwell's equations [5], the fluid-structure interaction problem [20, 22, 23, 43], and the scattering problem [38].

From a geometric perspective, this method has been used for flat unbounded interfaces [5, 16, 17, 26, 31, 35, 38], circular interfaces [18, 19], cylindrical interfaces [21–23, 43], and spherical interfaces [22]. In this paper, we address for the three-dimensional (3D) case a flat interface that, unlike previous works on this topic, is not an unbounded surface. Rather, we consider here the case of a flat circular interface arising when cylindrical geometries are coupled along the axial direction. Analogously, for the overlapping case, the interface region is given here by a cylinder instead of a 3D strip.

The study of circular flat interfaces is of particular interest when a Partial Differential Equation (PDE) is solved in a cylindrical domain which is split in two (or more) cylinders with interfaces orthogonal to the axial

Keywords and phrases. Optimized Schwarz Method, cylindrical domains, geometric multiscale, Bessel functions.

¹ Dipartimento di Ingegneria gestionale, dell'informazione e della produzione, Università degli Studi di Bergamo, Viale Marconi 5, 24044 Dalmine (BG), Italy.

² MOX, Dipartimento di Matematica, Politecnico di Milano, Piazza Leonardo da Vinci 32, 20133 Milan, Italy.

* Corresponding author: christian.vergara@polimi.it

direction. For example, this is the case when parallel computing is performed to speed up the numerical solution of the problem at hand, or for jumping material parameters. Here, we provide a convergence analysis of the partitioned procedure arising in this context for a diffusion-reaction problem, and we discuss some optimal choices of the interface parameters. We also show some numerical results that highlight the effectiveness of our theoretical findings, and highlight the relationship between the convergence and the Finite Element errors.

In the second part of the paper, we address the split of a cylinder into two non-overlapping cylinders, where one of them (let say the distal one) is substituted by a geometric reduced one-dimensional model, where only the axial coordinate survives. This leads to a *geometric multiscale* model, where the geometric heterogeneous coupling between 3D and 1D models is addressed. This coupled problem has been studied in a general framework in [2, 29], and widely considered in hemodynamic applications, see *e.g.* [4, 7, 33, 37]. The interface conditions appearing in partitioned algorithms for the 3D–1D coupled problem in hemodynamics involve Dirichlet and Neumann data [9], the total pressure [3, 10], or the characteristic variables [7]. Other type of partitioned algorithms were obtained in [4] by considering a Lagrange multipliers mortaring, and in [3, 29, 32] by introducing the interface equation. Here, we address the case of Robin-type interface conditions for the reaction-diffusion problem. In particular, we study the convergence of the resulting Schwarz method and we propose optimal values for the interface parameters. Finally, we show some numerical results highlighting the effectiveness of our theoretical findings.

The outline of this paper is as follows. In Section 2 we address the case of the generalized Schwarz algorithm obtained in the 3D–3D splitting, whereas in Section 3 the one arising from the 3D–1D coupling. For each of these two sections, we provide a convergence analysis of the related generalized Schwarz algorithm, we discuss possible optimization procedures to find effective values of the interface parameters, and we show the numerical results.

2. THE 3D–3D SPLITTING CASE

2.1. Problem setting

Referring to Figure 1, we consider the following coupled problem in the overlapping subdomains $\Omega_1 = \{(r, \varphi, z) : 0 \leq r < R, 0 \leq \varphi < 2\pi, -\infty < z < H\}$ and $\Omega_2 = \{(r, \varphi, z) : 0 \leq r < R, 0 \leq \varphi < 2\pi, 0 < z < +\infty\}$

$$-\mu_1 \Delta u_1 + \gamma_1 u_1 = f_1 \quad \mathbf{x} \in \Omega_1, \quad (2.1a)$$

$$u_1|_{\Sigma} = u_1|_{z \rightarrow -\infty} = 0, \quad (2.1b)$$

$$u_1 = u_2 \quad \mathbf{x} \in \Gamma_1, \quad (2.1c)$$

$$\mu_1 \frac{\partial u_1}{\partial z} = \mu_2 \frac{\partial u_2}{\partial z} \quad \mathbf{x} \in \Gamma_2, \quad (2.1d)$$

$$-\mu_2 \Delta u_2 + \gamma_2 u_2 = f_2 \quad \mathbf{x} \in \Omega_2, \quad (2.1e)$$

$$u_2|_{\Sigma} = u_2|_{z \rightarrow \infty} = 0, \quad [-6pt] \quad (2.1f)$$

where $\mu_1, \mu_2, \gamma_1, \gamma_2$ are given positive parameters, f_1 and f_2 given functions, Σ is the lateral surface, and we considered the homogeneous case in view of the convergence analysis. The interfaces Γ_1 and Γ_2 are located at $z = H \geq 0$ and $z = 0$, respectively. Notice that in the non-overlapping case we could have $\mu_1 \neq \mu_2$ and $\gamma_1 \neq \gamma_2$, due to a jump of the coefficients representing two different media located in Ω_1 and Ω_2 , respectively. In the overlapping case, of course we should have $\mu_1 = \mu_2$ and $\gamma_1 = \gamma_2$ in $\Omega_1 \cap \Omega_2$. However, for the sake of generality, we consider the general framework given by (2.1) also in the overlapped case.

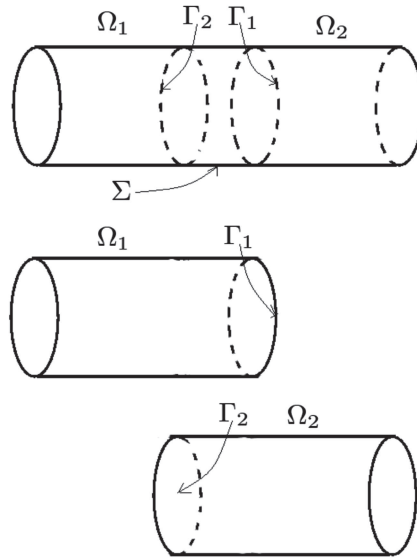


FIGURE 1. Unsplit computational domain (*up*) and overlapping subdomains (*bottom*).

Introducing two linear operators $\mathcal{S}_1 \neq \mathcal{S}_2$, we consider the following *generalized Schwarz* method for the solution of the previous problem, obtained by linearly combining the interface equations (2.1c) and (2.1d): Given $u_2^{(0)}$, at each iteration $n > 0$, until convergence

1. solve the problem in Ω_1 :

$$-\mu_1 \Delta u_1^{(n)} + \gamma_1 u_1^{(n)} = f_1 \quad \mathbf{x} \in \Omega_1, \tag{2.2a}$$

$$u_1^{(n)}|_{\Sigma} = u_1^{(n)}|_{z \rightarrow -\infty} = 0, \tag{2.2b}$$

$$\mathcal{S}_1 u_1^{(n)} + \mu_1 \frac{\partial u_1^{(n)}}{\partial z} = \mathcal{S}_1 u_2^{(n-1)} + \mu_2 \frac{\partial u_2^{(n-1)}}{\partial z} \quad \mathbf{x} \in \Gamma_1; \tag{2.2c}$$

2. solve the problem in Ω_2 :

$$-\mu_2 \Delta u_2^{(n)} + \gamma_2 u_2^{(n)} = f_2 \quad \mathbf{x} \in \Omega_2, \tag{2.3a}$$

$$u_2^{(n)}|_{\Sigma} = u_2^{(n)}|_{z \rightarrow \infty} = 0, \tag{2.3b}$$

$$\mathcal{S}_2 u_2^{(n)} + \mu_2 \frac{\partial u_2^{(n)}}{\partial z} = \mathcal{S}_2 u_1^{(n)} + \mu_1 \frac{\partial u_1^{(n)}}{\partial z} \quad \mathbf{x} \in \Gamma_2. \tag{2.3c}$$

2.2. Convergence analysis

We report in what follows a convergence result of the previous partitioned algorithm. In this first analysis, we assume that u_1 and u_2 do not depend on the angular coordinate φ , *i.e.* $u_j = u_j(r, z)$, $j = 1, 2$. Although simplified, the following analysis will highlight important features of the coupling with a flat circular interface in presence of cylindrical geometries. As usual, due the linearity of the problem, we consider the homogenous case, *i.e.* $f_1 = f_2 = 0$, and study the convergence of the iterative algorithm with a non zero initial guess.

The main tool in this convergence analysis consists in expanding all functions defined on the circular cross sections $z = z_0$ of the cylinder with respect to the eigenfunctions of the 2D Laplacian on the circle satisfying

Dirichlet homogeneous boundary conditions. The expression of the 2D Laplacian in polar coordinates is

$$\Delta w = \frac{1}{r} \frac{\partial}{\partial r} \left(r \frac{\partial w}{\partial r} \right) + \frac{1}{r^2} \frac{\partial^2 w}{\partial \varphi^2}.$$

In the radial case this reduces to

$$\Delta w = \frac{1}{r} \frac{\partial}{\partial r} \left(r \frac{\partial w}{\partial r} \right),$$

with eigenfunctions given by $J_0(\alpha r)$ and eigenvalues $-\alpha^2$, for any $\alpha \in \mathbb{R}$, where J_0 is the Bessel function of the first kind of order zero. The Bessel functions of the first kind of order ν , $\nu = 0, 1, \dots$, are analytic functions oscillating around the x -axis defined by

$$J_\nu(x) = \sum_{m=0}^{\infty} \frac{(-1)^m}{m!(m + \nu + 1)!} \left(\frac{x}{2}\right)^{2m+\nu}, \quad \nu = 0, 1, \dots,$$

see [27] for further details.

The homogeneous boundary conditions $w(R) = 0$ finally impose $\alpha = x_k/R$, $k = 1, 2, \dots$, where $\{x_k\}_{k=0}^{+\infty}$ are the positive zeros of J_0 , and R is the radius of the cylinder. It is a classic result that $\{J_0(x_k r/R)\}_{k=1}^{+\infty}$ is a complete orthogonal system of $L^2([0, R], r dr)$. Notice that the eigenfunctions of the 2D Laplacian are well known even in the non radial case, in particular they involve other Bessel functions in addition to J_0 (see e.g. [27], (6.3.14) p. 149).

Thus, the Fourier-Bessel expansion of functions u_1 and u_2 are given by

$$u_j(r, z) = \sum_{k=1}^{+\infty} \widehat{u}_j(k, z) J_0\left(x_k \frac{r}{R}\right), \quad j = 1, 2, \tag{2.4}$$

where

$$\widehat{u}_j(k, z) = \frac{2}{R^2 J_1(x_k)^2} \int_0^R u_j(r, z) J_0\left(x_k \frac{r}{R}\right) r dr, \quad j = 1, 2.$$

Notice that such functions satisfy the condition $u_j|_{\Sigma} = 0$.

It is well known, and indeed easy to show, that if the linear operators \mathcal{S}_j commute with the 2D Laplacian (for example when \mathcal{S}_j are just multiplications by a scalar, or differential operators), then they have the form

$$\mathcal{S}_j w(r, z) = \sum_{k=1}^{+\infty} \sigma_j(k) \widehat{w}(k, z) J_0\left(x_k \frac{r}{R}\right), \quad j = 1, 2,$$

and $\{\sigma_j(k)\}_{k=1}^{+\infty}$, $j = 1, 2$, are called symbols of \mathcal{S}_j related to the Fourier-Bessel expansion. When all $\sigma_j(k)$ are equal, and therefore \mathcal{S}_j is just multiplication by a scalar, we shall denote them simply by σ_j .

We have the following result.

Proposition 2.1. *The reduction factor related to the iterations (2.2) and (2.3), in the case $u_1 = u_1(r, z)$, $u_2 = u_2(r, z)$, is given by*

$$\rho_{3D-3D}(k) = \frac{\sigma_2(k) + \mu_1 \beta_{1,k}}{\sigma_2(k) - \mu_2 \beta_{2,k}} \cdot \frac{\sigma_1(k) - \mu_2 \beta_{2,k}}{\sigma_1(k) + \mu_1 \beta_{1,k}} e^{-(\beta_{1,k} + \beta_{2,k})H}, \tag{2.5}$$

where

$$\beta_{j,k} = \sqrt{\frac{\gamma_j}{\mu_j} + \frac{x_k^2}{R^2}}. \tag{2.6}$$

Proof. Since the expression of the Laplacian in cylindrical coordinates is

$$\Delta w = \frac{1}{r} \frac{\partial}{\partial r} \left(r \frac{\partial w}{\partial r} \right) + \frac{1}{r^2} \frac{\partial^2 w}{\partial \varphi^2} + \frac{\partial^2 w}{\partial z^2},$$

and since the eigenfunctions of

$$\frac{1}{r} \frac{\partial}{\partial r} \left(r \frac{\partial w}{\partial r} \right)$$

are the functions $J_0(\alpha r)$ with eigenvalues $-\alpha^2$, $\alpha \in \mathbb{R}$, we have for each $j = 1, 2$ owing to (2.4)

$$\begin{aligned} \Delta u_j &= \frac{1}{r} \frac{\partial}{\partial r} \left(r \frac{\partial u_j}{\partial r} \right) + \frac{\partial^2 u_j}{\partial z^2} \\ &= \sum_{k=1}^{+\infty} \widehat{u}_j(k, z) \frac{1}{r} \frac{\partial}{\partial r} \left(r \frac{\partial \left(J_0 \left(x_k \frac{r}{R} \right) \right)}{\partial r} \right) + \sum_{k=1}^{+\infty} \frac{\partial^2 \widehat{u}_j(k, z)}{\partial z^2} J_0 \left(x_k \frac{r}{R} \right) \\ &= \sum_{k=1}^{+\infty} \left(-\frac{x_k^2}{R^2} \right) \widehat{u}_j(k, z) J_0 \left(x_k \frac{r}{R} \right) + \sum_{k=1}^{+\infty} \frac{\partial^2 \widehat{u}_j(k, z)}{\partial z^2} J_0 \left(x_k \frac{r}{R} \right). \end{aligned}$$

The equations $\gamma_j u_j - \mu_j \Delta u_j = 0$ therefore become

$$\begin{aligned} \gamma_j \sum_{k=1}^{+\infty} \widehat{u}_j(k, z) J_0 \left(x_k \frac{r}{R} \right) - \mu_j \sum_{k=1}^{+\infty} \left(-\frac{x_k^2}{R^2} \right) \widehat{u}_j(k, z) J_0 \left(x_k \frac{r}{R} \right) - \mu_j \sum_{k=1}^{+\infty} \frac{\partial^2 \widehat{u}_j(k, z)}{\partial z^2} J_0 \left(x_k \frac{r}{R} \right) &= 0 \\ \sum_{k=1}^{+\infty} \left(\left(\frac{\gamma_j}{\mu_j} + \frac{x_k^2}{R^2} \right) \widehat{u}_j(k, z) - \frac{\partial^2 \widehat{u}_j(k, z)}{\partial z^2} \right) J_0 \left(x_k \frac{r}{R} \right) &= 0. \end{aligned}$$

This gives

$$\left(\frac{\gamma_j}{\mu_j} + \frac{x_k^2}{R^2} \right) \widehat{u}_j(k, z) - \frac{\partial^2 \widehat{u}_j(k, z)}{\partial z^2} = 0$$

for every $k = 1, 2, 3, \dots$. The condition $u_1|_{z=-\infty} = 0$ and $u_2|_{z=\infty} = 0$ give

$$\widehat{u}_1(k, z) = C_1(k) e^{\beta_{1,k} z} \quad \widehat{u}_2(k, z) = C_2(k) e^{-\beta_{2,k} z}, \quad (2.7)$$

where $\beta_{j,k}$ are given by (2.6) and $C_j(k)$, $j = 1, 2$, are two functions determined as usual by the interface conditions.

Now, by writing the Fourier-Bessel expansions of the interface conditions (2.2c) and (2.3c) and using (2.7), we obtain

$$(\sigma_1(k) + \mu_1 \beta_{1,k}) C_1^{(n)}(k) e^{\beta_{1,k} H} = (\sigma_1(k) - \mu_2 \beta_{2,k}) C_2^{(n-1)}(k) e^{-\beta_{2,k} H},$$

$$(\sigma_2(k) - \mu_2 \beta_{2,k}) C_2^{(n)}(k) = (\sigma_2(k) + \mu_1 \beta_{1,k}) C_1^{(n)}(k).$$

Taking as usual for the reduction factor to quantity $C_2^{(n)}(k)/C_2^{(n-1)}(k)$ (see *e.g.* [16]), we obtain the thesis. \square

Remark 2.2. As mentioned before, the analysis of the general case $u_j = u_j(r, z, \varphi)$ requires the use of other Bessel functions in addition to J_0 . Moreover, the extension of the previous analysis makes the subsequent optimization procedures somewhat involved. This is currently under investigation.

We consider now the case without overlap, $H = 0$. In this case, we can use the general convergence analysis provided in [22]. In particular, we have the following result.

Proposition 2.3. *In the case without overlap ($H=0$), iterations (2.2) and (2.3), with $u_1 = u_1(r, z)$, $u_2 = u_2(r, z)$, converge for a fixed value of k if and only if*

$$\begin{aligned} \sigma_2(k) < \sigma_1(k) \text{ and } \left(\sigma_1(k) + \frac{\mu_1\beta_{1,k} - \mu_2\beta_{2,k}}{2} \right) \left(\sigma_2(k) + \frac{\mu_1\beta_{1,k} - \mu_2\beta_{2,k}}{2} \right) < \left(\frac{\mu_1\beta_{1,k} + \mu_2\beta_{2,k}}{2} \right)^2, \text{ or} \\ \sigma_2(k) > \sigma_1(k) \text{ and } \left(\sigma_1(k) + \frac{\mu_1\beta_{1,k} - \mu_2\beta_{2,k}}{2} \right) \left(\sigma_2(k) + \frac{\mu_1\beta_{1,k} - \mu_2\beta_{2,k}}{2} \right) > \left(\frac{\mu_1\beta_{1,k} + \mu_2\beta_{2,k}}{2} \right)^2. \end{aligned}$$

Proof. Referring to Theorem 1 in [22], we observe that the hypothesis for its application are satisfied since $\mu_2\beta_{2,k} > -\mu_1\beta_{1,k}$ for all k , see [22]. Thus, the thesis follows by a straightforward application of this theorem. \square

2.3. Optimization procedures

We refer again to [22], where a general way to provide optimal values of the interface parameters in the case of constant symbols $\sigma_j(k) = \sigma_j$ is provided for the case without overlap. We report, for the sake of exposition, only the case $\mu_1 = \mu_2 = 1$. We introduce k_{\max} , the maximum value of k assumed to be relevant. Moreover, since k represents the index related to the roots x_k , in the practice we usually set $k_{\min} = 1$. We have the following result.

Proposition 2.4. *There exist three numbers $\rho_0 < 1$, p_- , p_+ , such that the reduction factor (2.5) for $H=0$ satisfies*

$$\rho_{3D-3D}(k) \leq \rho_0, \quad \forall k = k_{\min}, \dots, k_{\max},$$

provided that $\sigma_1 = p$, $\sigma_2 = 2M - p$, with $p \in [p_-, p_+]$ and $M = \frac{1}{2} \left(\sqrt{\gamma_2 + \frac{x_{k_{\min}}^2}{R^2}} - \sqrt{\gamma_1 + \frac{x_{k_{\min}}^2}{R^2}} \right)$. In particular, for the case $\gamma_1 = \gamma_2 = \gamma$, we have $M = 0$,

$$p_- = \frac{1 - \sqrt{\rho_0}}{1 + \sqrt{\rho_0}} \beta_{k_{\max}} \quad p_+ = \frac{1 + \sqrt{\rho_0}}{1 - \sqrt{\rho_0}} \beta_{k_{\min}}. \tag{2.8}$$

and

$$\rho_0 = \left(\frac{1 - \sqrt[4]{\frac{R^2\gamma + x_{k_{\min}}^2}{R^2\gamma + x_{k_{\max}}^2}}}{1 + \sqrt[4]{\frac{R^2\gamma + x_{k_{\min}}^2}{R^2\gamma + x_{k_{\max}}^2}}} \right)^2.$$

Proof. The thesis follows by the application of Theorem 2 in [22]. \square

The previous result gives us a range of constant values for the interface parameters which guarantees that the reduction factor is less than $\rho_0 < 1$, *i.e.* convergence independent of k .

In the case with overlap $H > 0$, specific optimization procedures should be considered which cannot be derived directly from Theorem 2 in [22]. This topic is under investigation.

2.4. Numerical results

2.4.1. Generalities

The numerical results presented here have been obtained by means of the Finite Element (FE) code *FreeFem++* (www.freefem.org).

In all the numerical experiments, we consider the cylinder $\Omega = \{(r, \varphi, z) : 0 \leq r < R, 0 \leq \varphi < 2\pi, 0 < z < 2L\}$ split into two non-overlapping domains $\Omega_1 = \{(r, \varphi, z) : 0 \leq r < R, 0 \leq \varphi < 2\pi, 0 < z < L\}$ and $\Omega_2 = \{(r, \varphi, z) : 0 \leq r < R, 0 \leq \varphi < 2\pi, L < z < 2L\}$, separated by the interface $\Gamma = \{(r, \varphi, z) : 0 \leq r < R, 0 \leq \varphi < 2\pi, z = L\}$. In our case, we have used $R=0.5$ and $L=2.5$. We prescribe homogeneous Dirichlet conditions

on $\partial\Omega_i \setminus \Gamma$, $i = 1, 2$. Moreover, if not otherwise specified, we set $\gamma_1 = \gamma_2 = 10$ and $\mu_1 = \mu_2 = 1$. As a consequence, we have $M = 0$ in the estimates of Proposition 2.4.

The numerical solutions have been obtained by solving two-dimensional axi-symmetric problems. The corresponding meshes were formed by triangles, and, if not otherwise specified, the discretization parameter is $h = R/10 = 0.05$.

For the sake of completeness, we report in what follows explicitly iterations (2.2) and (2.3) applied to our context:

Given the function $u_2^{(0)}$ and the real numbers σ_1 and σ_2 , at each iteration $n > 0$, until $\int_{\Gamma} |u_1^{(n)} - u_1^{(n-1)}|^2 d\gamma \geq \varepsilon^2$,

1. solve the problem in Ω_1 :

$$-\mu_1 \Delta u_1^{(n)} + \gamma_1 u_1^{(n)} = 0 \quad \mathbf{x} \in \Omega_1, \quad (2.9a)$$

$$u_1^{(n)} = 0 \quad \mathbf{x} \in \partial\Omega_1 \setminus \Gamma, \quad (2.9b)$$

$$\sigma_1 u_1^{(n)} + \mu_1 \frac{\partial u_1^{(n)}}{\partial z} = \sigma_1 u_2^{(n-1)} + \mu_2 \frac{\partial u_2^{(n-1)}}{\partial z} \quad \mathbf{x} \in \Gamma; \quad (2.9c)$$

2. solve the problem in Ω_2 :

$$-\mu_2 \Delta u_2^{(n)} + \gamma_2 u_2^{(n)} = 0 \quad \mathbf{x} \in \Omega_2, \quad (2.10a)$$

$$u_2^{(n)} = 0 \quad \mathbf{x} \in \partial\Omega_2 \setminus \Gamma = 0, \quad (2.10b)$$

$$\sigma_2 u_2^{(n)} + \mu_2 \frac{\partial u_2^{(n)}}{\partial z} = \sigma_2 u_1^{(n)} + \mu_1 \frac{\partial u_1^{(n)}}{\partial z} \quad \mathbf{x} \in \Gamma. \quad (2.10c)$$

We set $\varepsilon = 10^{-7}$. If not otherwise specified, we use P2 Finite Elements.

2.4.2. On the choice of the frequencies in the optimization procedure

In the above Proposition 2.4, the optimal interface parameters are established after an *a priori* evaluation of the relevant “frequency” parameters k . It is well known that when applying this method in a numerical simulation, certain frequencies can be considered irrelevant to the problem. For example, in the (two dimensional) classical approach to the problem, the interface is modeled as an unbounded line, and the continuous Fourier transform $\int_{-\infty}^{+\infty} f(x)e^{-ixm} dx$ is used. When adapting this analysis to a particular case, only the frequencies m between two values M_{\min} and M_{\max} are considered. Indeed, one can disregard all frequencies smaller than $M_{\min} = \pi/D$, where D is a characteristic dimension of the effective interface used in the numerical experiment, as well as all frequencies greater than the Nyquist–Shannon frequency $M_{\max} = \pi/h$. The Fourier-Bessel expansion that we use here already takes into account the shape and dimensions of the interface. Thus, unlike the case of analysis for an unbounded interface, there is no reason to disregard any of the lower values of the “frequency” parameter k . On the other hand, in our two-dimensional axi-symmetric numerical simulations the interface reduces to the interval $[0, R]$ and the mesh size is given by $h = R/N$ for an integer N , with nodes, say, $0 = r_1 < r_2 < \dots < r_N < r_{N+1} = R$. In this situation one can disregard all the values of k greater than N . Indeed, if $k > N$ then the linear system

$$\begin{cases} u_2^{(0)}(r_1, L) = \alpha_1 J_0\left(\frac{x_1 r_1}{R}\right) + \dots + \alpha_k J_0\left(\frac{x_k r_1}{R}\right) \\ \dots \\ u_2^{(0)}(r_N, L) = \alpha_1 J_0\left(\frac{x_1 r_N}{R}\right) + \dots + \alpha_k J_0\left(\frac{x_k r_N}{R}\right) \end{cases}$$

has more variables than equations, and therefore will never have one solution only (we have not considered the equation corresponding to $r_{N+1} = R$ since all the functions $J_0(x_k r/R)$ vanish there). For this reason, when

computing the optimal interface values in (2.8), all the values of k greater than $R/h = N$ can be considered irrelevant to the problem.

In conclusion, according to the previous analysis, the shape and dimension of the interface and the size of the mesh allow us to disregard all frequency parameters k outside the interval $[K_{\min}, K_{\max}]$, where $K_{\min} = 1$ and $K_{\max} = R/h$.

It is perhaps worth observing here that the value $K_{\max} = R/h = N$ corresponds to the Nyquist–Shannon frequency π/h in the following sense: the function $J_0\left(\frac{x_k r}{R}\right)$ with the highest possible value of k , that is $J_0\left(\frac{x_{Nr}}{R}\right)$, performs exactly N half oscillations in the interval $[0, R]$, which means on average half oscillation for each interval of length h . Similarly, the functions e^{imx} with the highest possible value of m , that is $e^{\pm i\pi x/h}$ perform exactly half oscillation for each interval of length h .

Thus, by the above observations, it is reasonable to assume that the initial guess takes the form

$$u_2^{(0)}(r, L) = \sum_{k=k_1}^{k_2} \widehat{u_2^{(0)}}(k) J_0\left(x_k \frac{r}{R}\right),$$

with $1 \leq k_1 \leq k_2 \leq K_{\max}$. From a theoretical (continuous) point of view, no other frequency appears in the iterative process other than those between k_1 and k_2 . For this reason the best possible choice in Proposition 2.4 should be $k_{\min} = k_1$ and $k_{\max} = k_2$.

In the practical (discrete) situation, however, as the iterations proceed, frequencies other than those strictly between k_1 and k_2 seem to appear, due probably to the Finite Elements approximation. These new frequencies are not irrelevant to the computations, and it may therefore be better to choose different values of k_{\min} and k_{\max} than k_1 and k_2 , respectively, when applying Proposition 2.4.

In order to be able to detect the above described phenomenon in the practical (discrete) situations, it is convenient to define the following *effective reduction factor*

$$\rho_h^{(n)} = \frac{\left(\int_{\Gamma} |u_1^{(n)} - u_1^{(n-1)}|^2 d\gamma\right)^{1/2}}{\left(\int_{\Gamma} |u_1^{(n-1)} - u_1^{(n-2)}|^2 d\gamma\right)^{1/2}}, \tag{2.11}$$

which is computable by the numerical experiments (it is in fact the ratio between two consecutive stopping criterium quantities). Notice that by the orthogonality of the functions $J_0\left(\frac{x_k r}{R}\right)$,

$$\rho_h^{(n)} = \left(\sum_{k=1}^{+\infty} (\rho_{3D-3D}(k))^2 w_k\right)^{1/2}, \tag{2.12}$$

where

$$w_k = \frac{\left|\widehat{u_1^{(n-1)}}(k) - \widehat{u_1^{(n-2)}}(k)\right|^2 \pi R^2 J_1^2(x_k)}{\int_{\Gamma} |u_1^{(n-1)} - u_1^{(n-2)}|^2 d\gamma}. \tag{2.13}$$

Thus, the effective reduction factor $\rho_h^{(n)}$ can be considered as a weighted $\ell^2\left(\mathbb{N}, \{w_k\}_{k=1}^{+\infty}\right)$ average of the reduction factor $\{\rho_{3D-3D}(k)\}_{k=1}^{+\infty}$. For a generic initial guess $u_2^{(0)}$, one can *a posteriori* deduce that the leading frequency in the increment $\left(\int_{\Gamma} |u_1^{(n-1)} - u_1^{(n-2)}|^2 d\gamma\right)^{1/2}$ is one of the values of k for which $\rho_h^{(n)} \approx \rho_{3D-3D}(k)$. Indeed, if $\rho_h^{(n)} \approx \rho_{3D-3D}(\bar{k})$ for some \bar{k} , then one can extrapolate that in (2.12), all the weights are negligible except for $w_{\bar{k}}$, and this means precisely that the \bar{k} th Fourier-Bessel coefficient of $u_1^{(n-1)} - u_1^{(n-2)}$ is sensibly bigger than the others.

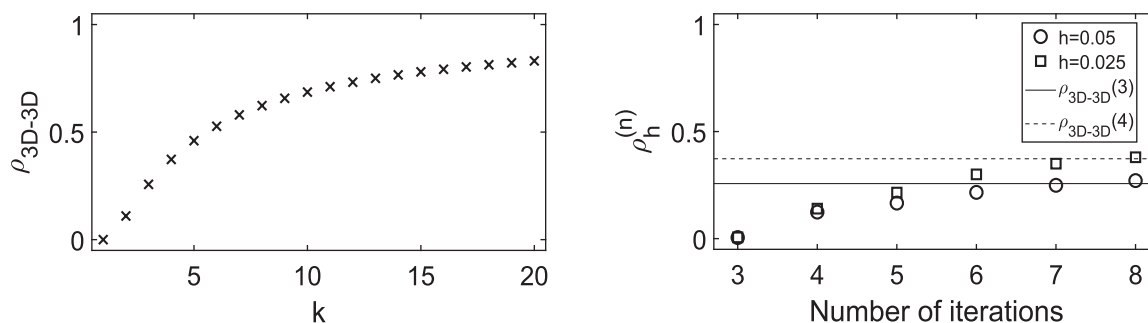


FIGURE 2. *Left*: estimated reduction factors as a function of k . *Right*: effective reduction factors as a function of the iteration n . For the latter plot, also the case obtained by halving the space discretization parameter is reported ($h=0.025$). The lines in the right figure represent the values of $\rho_{3D-3D}(3)$ and $\rho_{3D-3D}(4)$. Case $k_1 = k_2 = 1$ and $k_{\min} = k_{\max} = 1$.

In the forthcoming results, we will analyze the convergence history for different choices of k_1 , k_2 , k_{\min} and k_{\max} , all included in the range $[K_{\min}, K_{\max}] = [1, R/h]$. In order to make the exposition clearer, we recall that K_{\min} and K_{\max} are the extreme frequencies compatible with the mesh, k_1 and k_2 the extreme frequencies appearing in the initial guess, whereas k_{\min} and k_{\max} the extreme frequencies used in the application of (2.8) for the optimization.

2.4.3. $k_1 = k_2 = 1$

In the first set of numerical simulations, we consider in the initial guess only the first value of k , namely $k = 1$. Thus, in principle we should have $u_2^{(0)} = J_0\left(\frac{x_1 r}{R}\right)$. We want to investigate first the production of sources of error generated only by the FE error. Thus, we approximate $J_0\left(\frac{x_1 r}{R}\right)$ with a parabola, in order to have a vanishing projection error onto the FE space. In particular, we set

$$u_2^{(0)} = 1 - \left(\frac{r}{R}\right)^2.$$

Observe that the corresponding Fourier-Bessel coefficients $\hat{u}_2^{(0)}(k)$ from (2.13) are small for $k \neq 1$, but not vanishing. In particular, they decrease in modulus as k increases.

As a first choice, we set $k_{\min} = k_{\max} = 1$ in the optimization procedure, *i.e.* we exploit the fact that the main contribution in the initial guess is given by $k = 1$, thus ignoring the presence of other frequencies. Owing to the estimates (2.8), we obtain $p_- = p_+ = 5.75$. The numerical simulation converges in 8 iterations. In Figure 2 we report the reduction factors as a function of k estimated *a priori* by means of (2.5) and the effective reduction factors as a function of the number of the iteration n estimated by means of (2.11) (Notice that here and in the following figures, the effective reduction factor is reported, according to its definition (2.11), for $n \geq 3$).

From these results we observe that the *a priori* reduction factor in correspondence of $k = 1$ is as expected vanishing, and increasing values of ρ_{3D-3D} are obtained for increasing k . Notice that the effective reduction factor reaches a value which is very similar to $\rho_{3D-3D}(3) = 0.257$ indicated with a straight continuous line. This means that the leading value is $k = 3$. This is the result of the balance between small (large) values of the Fourier-Bessel coefficient for k large (small) and large (small) values of the corresponding ρ_{3D-3D} . In particular, although characterized by large values of the reduction factor (see Fig. 2, *left*) the high frequencies seem to not influence the convergence. Probably, also the FE error plays a role in determining the leading value of k , dumping and/or emphasizing some frequencies. This point is under investigation.

In order to investigate the effect of the mesh on these results, we have run the same test case for an halved value of h ($h = 0.025$). Since $k_1 = k_2 = 1$, we have the same values for ρ_{3D-3D} of above reported in Figure 2, *left*,

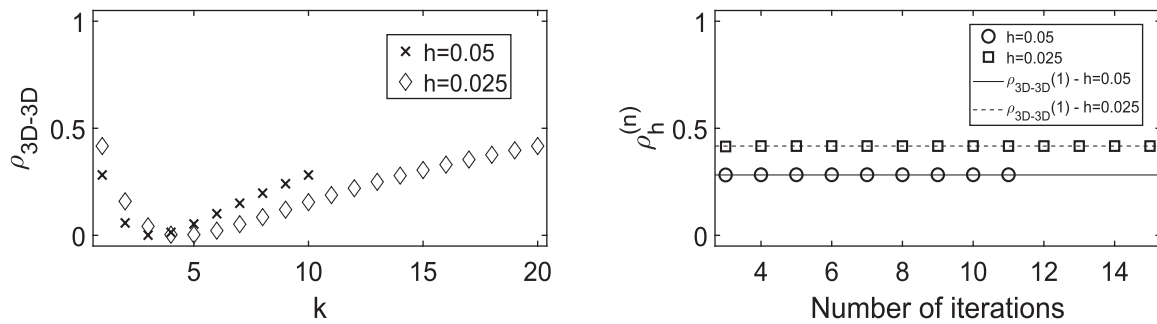


FIGURE 3. *Left*: estimated reduction factors as a function of k . *Right*: effective reduction factors as a function of the iteration n . The lines in the right figure represent the values of $\rho_{3D-3D}(1)$ obtained for the two values of h . Case $k_1 = k_2 = 1$ and $k_{\min} = 1$, $k_{\max} = 10$ ($k_{\max} = 20$ for $h = 0.025$).

and again $p_- = p_+ = 5.75$. In this case 9 iterations are needed to reach convergence. From the results reported in Figure 2, *right*, we observe that in this case the effective reduction factor reaches a value which is very similar to $\rho_{3D-3D}(4) = 0.373$, indicated with a straight dashed line. Thus, in this case the leading value is $k = 4$. We notice that in this case, also the values $k \in [11, 20]$ generated by the initial guess are “seen” by the numerical simulation, due to the decreased value of h . Higher values of the reduction factor ρ_{3D-3D} are associated to them, see Figure 2, *left*. Since the Fourier-Bessel coefficients in the initial guess corresponding to these values of k are small, but not vanishing, this justifies the increased number of iterations and of the leading value of k obtained for $h = 0.025$.

As a second choice, we set $k_{\min} = K_{\min} = 1$ and $k_{\max} = K_{\max} = R/h = 10$ in the optimization procedure, *i.e.* we ignore that the main contribution in the initial guess comes from $k = 1$ and we consider all the frequencies appearing in the initial guess. In this case, the estimates (2.8) lead to $p_- = p_+ = 18.79$. The numerical simulation converges in 11 iterations. In Figure 3 we report again the values of the reduction factors as a function of k estimated *a priori* by means of (2.5) and of the effective reduction factors as a function of the number of the iteration n estimated by means of (2.11).

From these results, first we observe that the *a priori* reduction factor given by the optimal choice (2.8) is not vanishing for $k = 1$. Instead, it features its maximum values for $k = 1$ and $k = 10$, that is the extreme values of the range of possible k 's. This is in accordance with the optimality procedure of Proposition 2.4 which is based on finding a range of constant (*i.e.* independent of k) values for the interface parameters that leads to a small reduction factor independently of k . Second, we highlight that this maximum value (0.282) is in fact coincident with the value reached by the effective reduction factor, see Figure 3, *right*. This means that $k = 1$ is the leading value of k in the practice computation (we exclude $k = 10$ since in the previous numerical computations we deduced that the higher frequencies, although characterized by large reduction factors, do not provide important contributions to the error). In this case, although an error due to $k = 2$ and $k = 3$ is still present (as in the previous case), it is rapidly dumped by the corresponding small reduction factor ($\rho_{3D-3D}(2) = 0.058$, $\rho_{3D-3D}(3) = 0.001$).

We ran the same test for a decreased value of h , namely $h = 0.025$. Thus, in this case we have $k_{\max} = 20$ and the values of the reduction factor ρ_{3D-3D} are not the same of above, see Figure 3, *left*. The number of iterations to reach convergence are in this case 15 and the leading value of k is again $k = 1$, corresponding to a value of the reduction factor equal to 0.417, see Figure 3, *right*. Again, the number of iterations and the value reached by the effective reduction factor are greater than in the case $h = 0.05$, only in this case this is due to the greater contribution of the reduction factor corresponding to the leading frequency $k = 1$ with respect to the case $h = 0.05$.

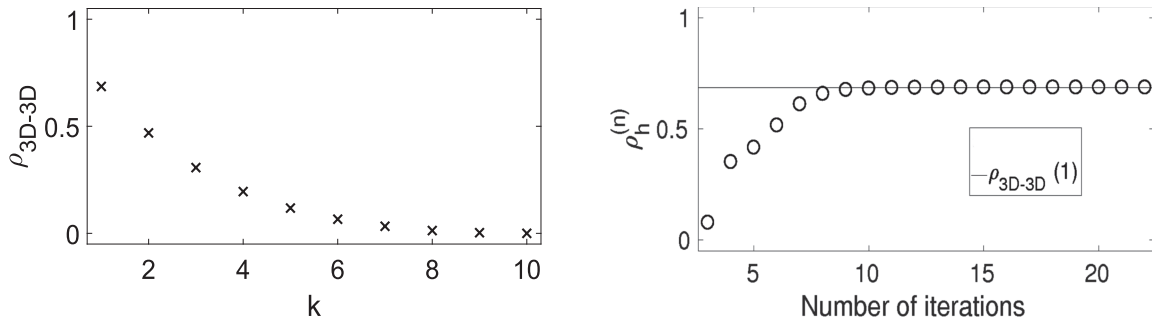


FIGURE 4. *Left*: estimated reduction factors as a function of k . *Right*: effective reduction factors as a function of the iteration n . The line in the right figure represents the value of $\rho_{3D-3D}(1)$. Case $k_1 = k_2 = 10$ and $k_{\min} = k_{\max} = 10$.

We repeated the same tests with initial guess

$$u_2^{(0)} = \frac{\sqrt{2}}{RJ_1(x_1)} J_0\left(\frac{x_1 r}{R}\right),$$

i.e. with only $k = 1$ at the beginning of the simulation. In the case $k_{\min} = k_{\max} = 1$ one should obtain convergence in one iteration, because $k = 1$ is the only frequency in the initial guess, and $\rho_{3D-3D} = 0.0$. In practice one obtains convergence in 7 iterations, with an effective reduction factor converging to $\rho_h^{(7)} = 0.300$ and a leading frequency between $k = 3$ and $k = 4$. This means that the projection onto the FE space introduces new frequencies that are not present in the initial guess. The results of the test with $k_{\min} = 1$ and $k_{\max} = 10$ are very similar to those obtained in the case of the parabola, with a clear leading frequency $k = 1$.

2.4.4. $k_1 = k_2 = 10$

In the second set of numerical simulations, we consider in the initial guess only the value $k = 10$. Thus, we set

$$u_2^{(0)} = \frac{\sqrt{2}}{RJ_1(x_{10})} J_0\left(\frac{x_{10} r}{R}\right).$$

As a first choice, we set $k_{\min} = k_{\max} = 10$ in the optimization procedure. Owing to the estimates (2.8), we obtain $p_- = p_+ = 61.35$. The numerical simulation converges in 22 iterations. In Figure 4 we report the reduction factors as a function of k estimated *a priori* by means of (2.5) and the effective reduction factors as a function of the number of the iteration n estimated by means of (2.11).

As expected, in this case the *a priori* reduction factor is vanishing for $k = 10$ and assumes increasing values for k decreasing. Again, we should expect convergence in one iteration. However, the presence of error sources due to the low values of k slows down the convergence, which is even slower than the previous case since the *a priori* reduction factors are higher. In particular, the effective reduction factor reaches a value that is in fact equal to $\rho_{3D-3D}(1) = 0.686$, see Figure 4, *right*. Thus, the leading value is $k = 1$.

As a second choice, we set $k_{\min} = 1$ and $k_{\max} = R/h = 10$ in the optimization procedure, *i.e.* we ignore that only $k = 10$ appears in the initial guess and we consider all the values of k predicted by the Shannon theorem. Of course, the estimates (2.8) lead again to $p_- = p_+ = 18.79$. The numerical simulation converges in 11 iterations. The values of the *a priori* reduction factor coincide by construction with those reported in Figure 3, *left*. The values of the effective reduction factors are in principle different, but in practice they coincide for $n \geq 4$ with those reported in Figure 3, *right*. Again, the leading value is $k = 1$, but the convergence is faster with respect to the previous case ($k_{\min} = k_{\max} = 10$) since $\rho_{3D-3D}(1)$ is smaller. This is a consequence of having included all

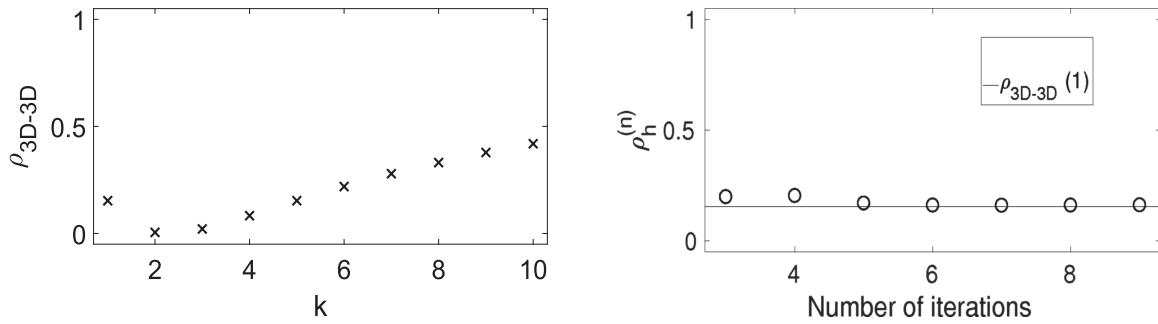


FIGURE 5. *Left*: estimated reduction factors as a function of k . *Right*: effective reduction factors as a function of the iteration n . The line in the right figure represents the value of $\rho_{3D-3D}(1)$. Case $k_1 = k_2 = 10$ and $k_{\min} = 1$, $k_{\max} = 5$.

the values of k in the optimization procedure, thus helping to dump the errors due to the small values of k introduced by the FE error.

As a third choice, we set $k_{\min} = 1$ and $k_{\max} = (R/h)/2 = 5$ in the optimization procedure, *i.e.* we consider only the smallest values of k among those allowed by the Shannon theorem. The estimates (2.8) lead to $p_- = p_+ = 13.14$. The numerical simulation converges in 9 iterations. In Figure 5 we report the reduction factors as a function of k estimated *a priori* by means of (2.5) and the effective reduction factors as a function of the number of the iteration n estimates by means of (2.11).

Interestingly, in this case the number of iterations is the lowest one among the three choices of k_{\min} and k_{\max} and the effective reduction factor tends to a value which is in fact very similar to $\rho_{3D-3D}(1) = 0.153$, see Figure 5, *right* (notice that in this case by construction $\rho_{3D-3D}(1) = \rho_{3D-3D}(5)$ and the optimization procedure produces higher values of the *a priori* reduction factor for $k \geq 6$). The reason of this improvement should be ascribed to the projection error of the initial guess onto the FE space (P2 in this case). Indeed, if $u_2^{(0)}$ was well projected, the error corresponding to $k = 10$ (the only frequency present in the initial guess) should slow down the convergence with an effective reduction factor close to $\rho_{3D-3D}(10) = 0.419$. The same arguments hold true for the numerical errors corresponding to $6 \leq k \leq 9$, since the corresponding *a priori* reduction factors are greater than $\rho_{3D-3D}(1)$. Probably, the projection error of the initial guess onto the P2 Finite Elements subspace dumps the contribution of the higher values of k . To confirm these observations, we run the same test as above with P3 FE. In this case, we need 12 iterations to reach convergence for the case $k_{\min} = 1$, $k_{\max} = 10$, with an effective reduction factor approaching the value 0.294, and 13 iterations for the case $k_{\min} = 1$, $k_{\max} = 5$, with an effective reduction factor approaching the value 0.329. Thus, the reduction of k_{\max} does not produce an improvement in the convergence, suggesting that in this case the smaller projection error does not dump the high values of k . In the latter case, the effective reduction factor reaches a value (0.329) similar to $\rho_{3D-3D}(8)$. Again, the contribution of the initial value $k = 10$ is dumped, but in this case the contribution corresponding to $k = 8$ is not.

2.4.5. $k_1 = 1$, $k_2 = 10$

In the third set of numerical simulations, we consider all the values of k compatible with the mesh in the initial guess, *i.e.* we set

$$u_2^{(0)} = \sum_{j=1}^{10} \frac{\sqrt{2}}{R J_1(x_j)} J_0\left(\frac{x_j r}{R}\right). \quad (2.14)$$

As a first choice, we set $k_{\min} = 1$, $k_{\max} = 10$ in the optimization procedure, *i.e.* $p_- = p_+ = 18.79$. The numerical simulation converges in 13 iterations. The effective reduction factor approaches the value 0.283 which is again very similar to $\rho_{3D-3D}(1)$ (see Fig. 3, *left*). As a second choice, we set $k_{\min} = 1$, $k_{\max} = 5$ in the optimization

TABLE 1. Values of M , ρ_0 and of the optimal range of p provided by the estimates reported in Proposition 2.4. Case $\gamma_1 = 100$, $\gamma_2 = 1$.

FE	k_{\min}	k_{\max}	M	ρ_0	p_-	p_+	# iter	$\rho_h^{(n_0)}$
P2	1	10	-3.09	0.22	19.08	19.13	$n_0 = 11$	0.22
P2	1	5	-3.09	0.10	12.46	12.57	$n_0 = 9$	0.22
P3	1	10	-3.09	0.22	19.08	19.13	$n_0 = 11$	0.22
P3	1	5	-3.09	0.10	12.46	12.57	$n_0 = 12$	0.26

procedure, *i.e.* $p_- = p_+ = 13.14$. Again, the number of iterations to reach convergence decreases (10) and the effective reduction factor approaches a value (0.165) very similar to $\rho_{3D-3D}(1)$ (see Fig. 5, *left*).

These results confirm that the projection error dumps the contribution of the highest values of k . Accordingly, one could think to improve the convergence by considering only $k=1$ in the optimization procedure, *i.e.* by setting $p_- = p_+ = 5.75$ (see Sect. 2.4.1). By doing so, the number of iterations to reach convergence is 16, with an effective reduction factor reaching the value 0.37, very similar to $\rho_{3D-3D}(4)$ (see Fig. 2, *left*). This means that we cannot reduce too much k_{\max} since low values of $k > 1$ give an important contribution to the error as a consequence of the FE error.

Once again, we run the same test with P3 FE. In this case, we need 13 iterations to reach convergence for the case $k_{\min} = 1$, $k_{\max} = 10$, with an effective reduction factor approaching the value 0.284, and 13 iterations for the case $k_{\min} = 1$, $k_{\max} = 5$, with an effective reduction factor approaching the value 0.321, similar to $\rho_{3D-3D}(8)$, see Figure 5, *left*. Again, the contribution of the initial value $k = 10$ is dumped, but the contribution corresponding to $k = 8$ is not. Thus, also in this case, for P3 FE the reduction of k_{\max} does not produce an improvement of the convergence.

Remark 2.5. We notice that in practical scenarios, the non-vanishing data (forcing term, Neumann and Dirichlet data) may introduce in the iteration procedure other frequencies in addition to those characterizing the initial guess. So, in principle the choice $k_{\min} = 1$, $k_{\max} = K_{\max}$ should be the most suitable for an effective optimization of the interface parameters owing to Proposition 2.4, since it accounts for all the possible frequencies. Here, we were interested in investigating what happens in the homogeneous case, in particular to study the effect of other frequencies, not generated by the non-vanishing data and not included in the initial guess, that emerged during the iterations.

2.4.6. The case of discontinuous coefficients

We address here the case $\gamma_1 = 100$, $\gamma_2 = 1$ and we consider as initial guess the function reported in (2.14), that is a function presenting the whole range of frequencies from $K_{\min} = 1$ to $K_{\max} = R/h = 10$. Referring to the quantities defined in Section 2.3, in Table 1 we report the results of the numerical experiments (for the definition of p_- and p_+ in the case $\gamma_1 \neq \gamma_2$ we refer to [22]).

From these results, we observe that the range of optimal p predicted by Proposition 2.4 is very thin, thus in fact providing directly the optimal value of p also in the case of discontinuous coefficients. The same type of phenomenon described in the case of continuous coefficients can be observed here too. The projection of the initial guess onto the Finite Element space P2 cancels the higher frequencies, and this gives a better performance when one takes $k_{\max} = 5$. On the other hand, when the P3 Finite Elements are used, the higher frequencies remain relevant to the problem and things behave as expected.

3. THE 3D-1D SPLITTING CASE

As observed in the Introduction, in some applications there is the need to couple a 3D problem with the corresponding reduced 1D model. In particular, referring to Figure 6 and to the notation of Section 2 and setting

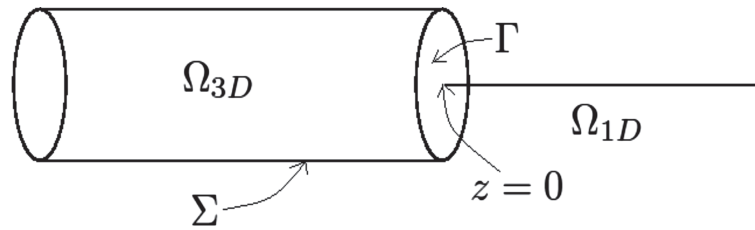


FIGURE 6. 3D–1D coupled subdomains.

$\Omega_{3D} = \Omega_1$, we consider the following coupled problem:

$$-\Delta u_{3D} + \gamma u_{3D} = f_{3D} \quad \mathbf{x} \in \Omega_{3D}, \tag{3.1a}$$

$$u_{3D}|_{\Sigma} = u_{3D}|_{z \rightarrow -\infty} = 0, \tag{3.1b}$$

$$\frac{1}{|\Gamma|} \int_{\Gamma} u_{3D} d\gamma = u_{1D}|_{z=0}, \tag{3.1c}$$

$$\frac{1}{|\Gamma|} \int_{\Gamma} \frac{\partial u_{3D}}{\partial z} d\gamma = \frac{\partial u_{1D}}{\partial z} \Big|_{z=0}, \tag{3.1d}$$

$$-\frac{\partial^2 u_{1D}}{\partial z^2} + \gamma u_{1D} = f_{1D} \quad z > 0, \tag{3.1e}$$

$$u_{1D}|_{z \rightarrow \infty} = 0, \tag{3.1f}$$

where we have located the point $z = 0$ at the 3D–1D interface and f_{3D} and f_{1D} are given functions.

For the solution of the previous problem, we consider again a generalized Schwarz method obtained by linearly combining the interface conditions (3.1c) and (3.1d) (notice that in this case the linear operators \mathcal{S}_{3D} and \mathcal{S}_{1D} are just multiplicative constants, and therefore coincide with their symbols σ_{3D} and σ_{1D} respectively):

Given $u_{1D}^{(0)}$, at each iteration $n > 0$, until convergence

1. solve the 3D problem in Ω_{3D} :

$$-\Delta u_{3D}^{(n)} + \gamma u_{3D}^{(n)} = f_{3D} \quad \mathbf{x} \in \Omega_{3D}, \tag{3.2a}$$

$$u_{3D}^{(n)}|_{\Sigma} = u_{3D}^{(n)}|_{z \rightarrow -\infty} = 0, \tag{3.2b}$$

$$\mathcal{S}_{3D} \frac{1}{|\Gamma|} \int_{\Gamma} u_{3D}^{(n)} d\gamma + \frac{1}{|\Gamma|} \int_{\Gamma} \frac{\partial u_{3D}^{(n)}}{\partial z} d\gamma = \mathcal{S}_{3D} \left(u_{1D}^{(n-1)} \Big|_{z=0} \right) + \frac{\partial u_{1D}^{(n-1)}}{\partial z} \Big|_{z=0}; \tag{3.2c}$$

2. solve the problem in Ω_{1D} :

$$-\frac{\partial^2 u_{1D}^{(n)}}{\partial z^2} + \gamma u_{1D}^{(n)} = f_{1D} \quad z > 0, \tag{3.3a}$$

$$u_{1D}^{(n)}|_{z \rightarrow \infty} = 0, \tag{3.3b}$$

$$\mathcal{S}_{1D} \left(u_{1D}^{(n)} \Big|_{z=0} \right) + \frac{\partial u_{1D}^{(n)}}{\partial z} \Big|_{z=0} = \mathcal{S}_{1D} \frac{1}{|\Gamma|} \int_{\Gamma} u_{3D}^{(n)} d\gamma + \frac{1}{|\Gamma|} \int_{\Gamma} \frac{\partial u_{3D}^{(n)}}{\partial z} d\gamma. \tag{3.3c}$$

Remark 3.1. We observe that the solution of the 3D problem (3.2) is not uniquely defined, since condition (3.2c) is *defective*, providing only one global information rather than one for each $\mathbf{x} \in \Gamma$. The numerical solution of defective problems has been intensively addressed *e.g.* in [6, 8, 11–15, 24, 28, 34, 36, 39–42, 44], where suitable

strategies to complete these conditions have been studied. In the numerical solution reported below, we made the following concrete choice to prescribe condition (3.2c):

$$\mathcal{S}_{3D} u_{3D}^{(n)} + \frac{\partial u_{3D}^{(n)}}{\partial z} = \mathcal{S}_{3D} \left(u_{1D}^{(n-1)} \Big|_{z=0} \right) + \frac{\partial u_{1D}^{(n-1)}}{\partial z} \Big|_{z=0}, \quad \mathbf{x} \in \Gamma. \quad (3.4)$$

3.1. Convergence analysis

We report in what follows a convergence analysis of the 3D–1D coupled problems (3.2) and (3.3). Again, we assume for the 3D solution independence of the angular variable and we set $f_{3D} = f_{1D} = 0$. We have the following result.

Proposition 3.2. *The reduction factor related to iterations (3.2) and (3.3), in the case $u_{3D} = u_{3D}(r, z)$, is given by*

$$\rho_{3D-1D} = \sum_{k=1}^{\infty} \frac{4}{x_k^2} \frac{(\sigma_{1D} + \beta_k)(\sigma_{3D} - \sqrt{\gamma})}{(\sigma_{1D} - \sqrt{\gamma})(\sigma_{3D} + \beta_k)},$$

with

$$\beta_k = \sqrt{\gamma + \frac{x_k^2}{R^2}}. \quad (3.5)$$

Proof. Referring to Section 2.2, we have that the solution of the 3D problems (3.1a) and (3.1b) is given by

$$u_{3D}(r, z) = \sum_{k=1}^{+\infty} \widehat{u}_{3D}(k, z) J_0\left(x_k \frac{r}{R}\right),$$

where the Fourier-Bessel coefficient is given by

$$\widehat{u}_{3D}(k, z) = C_{3D}(k) e^{\beta_k z},$$

with β_k given by (3.5). Instead, the 1D problems (3.1e) and (3.1f) is quickly solved by

$$u_{1D}(z) = C_{1D} e^{-\sqrt{\gamma} z}.$$

The application of the Fourier-Bessel expansion to the left-hand side of (3.4) and to the right-hand side (3.3c) leads to

$$\mathcal{S}_{3D} u_{3D}^{(n)}(r, 0) + \frac{\partial u_{3D}^{(n)}}{\partial z}(r, 0) = \sum_{k=1}^{\infty} (\sigma_{3D} + \beta_k) C_{3D}^{(n)}(k) J_0\left(x_k \frac{r}{R}\right) \quad (3.6)$$

and to

$$\begin{aligned} & \frac{\mathcal{S}_{1D}}{|\Gamma|} \int_{\Gamma} u_{3D}^{(n)} d\gamma + \frac{1}{|\Gamma|} \int_{\Gamma} \frac{\partial u_{3D}^{(n)}}{\partial z} d\gamma \\ &= \frac{2}{R^2} \sum_{k=1}^{+\infty} \left(\sigma_{1D} \int_0^R C_{3D}^{(n)}(k) J_0\left(x_k \frac{r}{R}\right) r dr + \int_0^R C_{3D}^{(n)}(k) \left(\frac{\partial}{\partial z} e^{\beta_k z} \right) \Big|_{z=0} J_0\left(x_k \frac{r}{R}\right) r dr \right) \\ &= \frac{2}{R^2} \sum_{k=1}^{+\infty} \left((\sigma_{1D} + \beta_k) C_{3D}^{(n)}(k) \int_0^R J_0\left(x_k \frac{r}{R}\right) r dr \right) \\ &= \sum_{k=1}^{+\infty} (\sigma_{1D} + \beta_k) C_{3D}^{(n)}(k) \frac{2J_1(x_k)}{x_k}, \end{aligned} \quad (3.7)$$

where the last identity follows from the formula $\frac{d}{dx}(xJ_0(x)) = xJ_1(x)$, see ([27], p. 103). For $X = 1, 3$ and for u_{XD}^n we obtain

$$\mathcal{S}_{XD} \left(u_{1D}^{(n)} \Big|_{z=0} \right) + \frac{\partial u_{1D}^{(n)}}{\partial z} \Big|_{z=0} = (\sigma_{XD} - \sqrt{\gamma}) C_{XD}^{(n)}.$$

Owing to the previous identity and to (3.6) and (3.7), the Robin interface conditions (3.4) and (3.3c) become

$$\sum_{k=1}^{\infty} (\sigma_{3D} + \beta_k) C_{3D}^{(n)}(k) J_0 \left(x_k \frac{r}{R} \right) = (\sigma_{3D} - \sqrt{\gamma}) C_{1D}^{(n-1)} = (\sigma_{3D} - \sqrt{\gamma}) C_{1D}^{(n-1)} \sum_{k=1}^{\infty} \frac{2}{J_1(x_k)x_k} J_0 \left(x_k \frac{r}{R} \right)$$

which becomes

$$(\sigma_{3D} + \beta_k) C_{3D}^{(n)}(k) = (\sigma_{3D} - \sqrt{\gamma}) C_{1D}^{(n-1)} \frac{2}{J_1(x_k)x_k},$$

and

$$\sum_{k=1}^{\infty} (\sigma_{1D} + \beta_k) C_{3D}^{(n)}(k) \frac{2J_1(x_k)}{x_k} = (\sigma_{1D} - \sqrt{\gamma}) C_{1D}^{(n)}.$$

This gives

$$\frac{C_{1D}^{(n)}}{C_{1D}^{(n-1)}} = \sum_{k=1}^{\infty} \frac{4}{x_k^2} \frac{(\sigma_{1D} + \beta_k)(\sigma_{3D} - \sqrt{\gamma})}{(\sigma_{1D} - \sqrt{\gamma})(\sigma_{3D} + \beta_k)}$$

and the thesis follows. □

3.2. Optimization procedures

First of all, we notice that the choice $\sigma_{3D} = \sigma_{3D}^{\text{opt}} = \sqrt{\gamma}$ gives $\rho_{3D-1D} = 0$, and therefore convergence in two steps.

In order to fix an effective value for σ_{1D} for all the relevant k , we propose the following argument. Due to the source of error introduced by the numerical discretization of the two subproblems, at the discrete level the optimal choice of σ_{3D} may differ from the exact value of $\sqrt{\gamma}$ by a small quantity ε . Thus assume

$$\sigma_{3D} = \sqrt{\gamma} + \varepsilon.$$

This gives

$$\rho_{3D-1D} = \sum_{k=1}^{\infty} \frac{4}{x_k^2} \frac{\sigma_{1D} + \beta_k}{(\sigma_{1D} - \sqrt{\gamma})(\sqrt{\gamma} + \varepsilon + \beta_k)} \varepsilon.$$

When $\varepsilon \rightarrow 0$, each term

$$\frac{\sigma_{1D} + \beta_k}{(\sigma_{1D} - \sqrt{\gamma})(\sqrt{\gamma} + \varepsilon + \beta_k)} \varepsilon$$

is asymptotic to

$$\frac{\sigma_{1D} + \beta_k}{(\sigma_{1D} - \sqrt{\gamma})(\sqrt{\gamma} + \beta_k)} \varepsilon.$$

Our goal is now to search for the value of σ_{1D} that minimizes the maximum value

$$\max_{\beta_k \in [\beta_{k_{\min}}, \beta_{k_{\max}}]} \left| \frac{\sigma_{1D} + \beta_k}{(\sigma_{1D} - \sqrt{\gamma})(\sqrt{\gamma} + \beta_k)} \right|.$$

Observe that

$$\begin{aligned} & \max_{\beta_k \in [\beta_{k_{\min}}, \beta_{k_{\max}}]} \left| \frac{\sigma_{1D} + \beta_k}{(\sigma_{1D} - \sqrt{\gamma})(\sqrt{\gamma} + \beta_k)} \right| = \max_{\beta_k \in [\beta_{k_{\min}}, \beta_{k_{\max}}]} \left| \frac{1}{\sqrt{\gamma} + \beta_k} - \frac{1}{\sqrt{\gamma} - \sigma_{1D}} \right| \\ &= \max_{y \in \left[\frac{1}{\beta_{k_{\max}} + \sqrt{\gamma}}, \frac{1}{\beta_{k_{\min}} + \sqrt{\gamma}} \right]} \left| y - \frac{1}{\sqrt{\gamma} - \sigma_{1D}} \right| \\ &= \begin{cases} \frac{1}{\beta_{k_{\min}} + \sqrt{\gamma}} - \frac{1}{\sqrt{\gamma} - \sigma_{1D}} & \text{if } \frac{1}{\sqrt{\gamma} - \sigma_{1D}} \leq \frac{1}{2} \left(\frac{1}{\beta_{k_{\max}} + \sqrt{\gamma}} + \frac{1}{\beta_{k_{\min}} + \sqrt{\gamma}} \right) \\ -\frac{1}{\beta_{k_{\max}} + \sqrt{\gamma}} + \frac{1}{\sqrt{\gamma} - \sigma_{1D}} & \text{if } \frac{1}{\sqrt{\gamma} - \sigma_{1D}} \geq \frac{1}{2} \left(\frac{1}{\beta_{k_{\max}} + \sqrt{\gamma}} + \frac{1}{\beta_{k_{\min}} + \sqrt{\gamma}} \right). \end{cases} \end{aligned}$$

Clearly, the value of σ_{1D} that minimizes the above quantity is the one for which

$$\frac{1}{\sqrt{\gamma} - \sigma_{1D}} = \frac{1}{2} \left(\frac{1}{\beta_{k_{\max}} + \sqrt{\gamma}} + \frac{1}{\beta_{k_{\min}} + \sqrt{\gamma}} \right) = \frac{\beta_{k_{\min}} + \beta_{k_{\max}} + 2\sqrt{\gamma}}{2(\beta_{k_{\max}} + \sqrt{\gamma})(\beta_{k_{\min}} + \sqrt{\gamma})},$$

that is

$$\sigma_{1D}^{\text{opt}} = \sqrt{\gamma} - \frac{2(\beta_{k_{\max}} + \sqrt{\gamma})(\beta_{k_{\min}} + \sqrt{\gamma})}{\beta_{k_{\min}} + \beta_{k_{\max}} + 2\sqrt{\gamma}}. \quad (3.8)$$

This gives the asymptotic (when $\beta_{k_{\min}} \neq \beta_{k_{\max}}$), as $\varepsilon \rightarrow 0$,

$$\rho_{3D-1D} \sim \left(\frac{1}{\beta_{k_{\min}} + \sqrt{\gamma}} - \frac{1}{\beta_{k_{\max}} + \sqrt{\gamma}} \right) \left(\sum_{k=k_{\min}}^{k_{\max}} \frac{2}{x_k^2} \right) \varepsilon = \frac{\beta_{k_{\max}} - \beta_{k_{\min}}}{(\beta_{k_{\min}} + \sqrt{\gamma})(\beta_{k_{\max}} + \sqrt{\gamma})} \left(\sum_{k=k_{\min}}^{k_{\max}} \frac{2}{x_k^2} \right) \varepsilon.$$

Notice that if only one frequency is involved (*i.e.* $\beta_{k_{\min}} = \beta_{k_{\max}} = \beta$), the optimal value (3.8) reduces to $\sigma_{1D}^{\text{opt}} = -\beta$ and from the previous estimate of the reduction factor, we have $\rho_{3D-1D} = 0$.

3.3. Numerical results

The numerical results for the 3D part have been obtained by means of *FreeFem++*, whereas the 1D ones with *Matlab*. The results have been post-processed for a “manual” coupling at each iteration. We have considered $\Omega_{3D} = \{(r, \varphi, z) : 0 \leq r < R, 0 \leq \varphi < 2\pi, -L < z < 0\}$, with $R = 1.0$ and $L = 2.5$, and $\Omega_{1D} = (0, L)$. The numerical solution in the 3D geometry has been obtained by solving a two-dimensional axi-symmetric problem in a rectangle. The corresponding meshes were formed by triangles. The stopping criterion corresponds to the residual of a block Gauss-Seidel scheme and it is given by (see [1]):

$$\left(\frac{1}{|I|} \int_{\Gamma} \left(\sigma_{3D} u_{3D}^{(n)} + \frac{\partial u_{3D}^{(n)}}{\partial z} \right) d\gamma - \sigma_{3D} u_{1D}^{(n)} - \frac{\partial u_{1D}^{(n)}}{\partial z} \right)^2 \leq \varepsilon^2,$$

where $\varepsilon = 10^{-5}$. We used P1 Finite Elements and we chose as initial guess $u_{1D}^{(0)} = 1$.

The value of the space discretization parameter was $h = 0.05$, so that the number of samples along the interface Γ was $N = 20$ and, according to Section 2.4, we set $k_{\min} = 1$ and $k_{\max} = 10$ (*i.e.* we account for the dumping of the projection). We considered two values of the reaction parameter, namely $\gamma = 1$ and $\gamma = 10$.

Referring to the quantities defined in Section 3.2, in Table 2 we report the results of the numerical experiments. In particular, for each scenario, we have considered four schemes: the Dirichlet-Neumann (DN, $\sigma_{3D} = +\infty, \sigma_{1D} = 0$), the Neumann-Dirichlet (ND, $\sigma_{3D} = 0, \sigma_{1D} = +\infty$), the Robin-Neumann (RN, $\sigma_{3D} = \sigma_{3D}^{\text{opt}}, \sigma_{1D} = 0$), and the Robin-Robin (RR, $\sigma_{3D} = \sigma_{3D}^{\text{opt}}, \sigma_{1D} = \sigma_{1D}^{\text{opt}}$) schemes.

TABLE 2. Values of σ_{3D}^{opt} and σ_{1D}^{opt} and number of iterations for the four schemes considered. X means no convergence achieved.

γ	σ_{3D}^{opt}	σ_{1D}^{opt}	# iter DN	# iter ND	# iter RN	# iter RR
1	1.00	-5.47	X	11	3	2
10	3.16	-8.63	X	19	4	3

We observe an excellent behavior of the Robin-based schemes in comparison with the classical ones. Moreover, the estimate provided by (3.8) seems to improve the convergence properties of the optimized Robin-Robin scheme with respect to the Robin-Neumann one.

Acknowledgements. CV has been partially supported by INDAM-GNCS, by the Italian MIUR PRIN12 project no. 201289A4LX “Modelli matematici e numerici del sistema cardiocircolatorio e loro applicazione in ambito clinico”, and by the H2020-MSCA-ITN-2017, EU project 765374 “ROMSOC – Reduced Order Modelling, Simulation and Optimization of Coupled systems”.

REFERENCES

- [1] S. Badia, F. Nobile and C. Vergara, Fluid-structure partitioned procedures based on Robin transmission conditions. *J. Comput. Phys.* **227** (2008) 7027–7051.
- [2] P. Blanco, M. Discacciati and A. Quarteroni, Modeling dimensionally-heterogeneous problems: analysis, approximation and applications. *Numer. Math.* **119** (2011) 299–335.
- [3] P.J. Blanco, S. Deparis and A.C.I. Malossi, On the continuity of mean total normal stress in geometrical multiscale cardiovascular problems. *J. Comput. Phys.* **51** (2013) 136–155.
- [4] P.J. Blanco, R.A. Feijóo and S.A. Urquiza, A unified variational approach for coupling 3d–1d models and its blood flow applications. *Comput. Methods Appl. Mech. Eng.* **196** (2007) 4391–4410.
- [5] V. Dolean, M.J. Gander and L. Gerardo Giorda, Optimized Schwarz Methods for Maxwell’s equations. *SIAM J. Sci. Comput.* **31** (2009) 2193–2213.
- [6] V.J. Ervin and H. Lee, Numerical approximation of a quasi-newtonian Stokes flow problem with defective boundary conditions. *SIAM J. Numer. Anal.* **45** (2007) 2120–2140.
- [7] L. Formaggia, J.-F. Gerbeau, F. Nobile and A. Quarteroni, On the coupling of 3D and 1D Navier–Stokes equations for flow problems in compliant vessels. *Comput. Methods Appl. Mech. Eng.* **191** (2001) 561–582.
- [8] L. Formaggia, J.-F. Gerbeau, F. Nobile and A. Quarteroni, Numerical treatment of defective boundary conditions for the Navier–Stokes equation. *SIAM J. Numer. Anal.* **40** (2002) 376–401.
- [9] L. Formaggia, A. Moura and F. Nobile, On the stability of the coupling of 3D and 1D fluid-structure interaction models for blood flow simulations. *ESAIM: M2AN* **41** (2007) 743–769.
- [10] L. Formaggia, A. Quarteroni and C. Vergara, On the physical consistency between three-dimensional and one-dimensional models in haemodynamics. *J. Comput. Phys.* **244** (2013) 97–112.
- [11] L. Formaggia, A. Veneziani and C. Vergara, A new approach to numerical solution of defective boundary value problems in incompressible fluid dynamics. *SIAM J. Numer. Anal.* **46** (2008) 2769–2794.
- [12] L. Formaggia, A. Veneziani and C. Vergara, Flow rate boundary problems for an incompressible fluid in deformable domains: formulations and solution methods. *Comput. Methods Appl. Mech. Eng.* **199** (2009) 677–688.
- [13] L. Formaggia and C. Vergara, Prescription of general defective boundary conditions in fluid-dynamics. *Milan J. Math.* **80** (2012) 333–350.
- [14] K. Galvin and H. Lee, Analysis and approximation of the cross model for quasi-newtonian flows with defective boundary conditions. *Appl. Math. Comp.* **222** (2013) 244–254.
- [15] K. Galvin, H. Lee and L.G. Rebholz, Approximation of viscoelastic flows with defective boundary conditions. *J. Non Newt. Fl. Mech.* **169–170** (2012) 104–113.
- [16] M.J. Gander, Optimized Schwarz methods. *SIAM J. Numer. Anal.* **44** (2006) 699–731.
- [17] M.J. Gander, F. Magoulès and F. Nataf, Optimized Schwarz methods without overlap for the Helmholtz equation. *SIAM J. Sci. Comput.* **24** (2002) 38–60.
- [18] M.J. Gander and Y. Xu, Optimized Schwarz methods for circular domain decompositions with overlap. *SIAM J. Numer. Anal.* **52** (2014) 1981–2004.
- [19] M.J. Gander and Y. Xu, Optimized Schwarz Methods with nonoverlapping circular domain decomposition. *Math. Comp.* **86** (2017) 637–660.

- [20] L. Gerardo Giorda, F. Nobile and C. Vergara, Analysis and optimization of Robin–Robin partitioned procedures in fluid-structure interaction problems. *SIAM J. Numer. Anal.* **48** (2010) 2091–2116.
- [21] G. Gigante, M. Pozzoli and C. Vergara, Optimized Schwarz methods for the diffusion-reaction problem with cylindrical interfaces. *SIAM J. Numer. Anal.* **51** (2013) 3402–3420.
- [22] G. Gigante and C. Vergara, Analysis and optimization of the generalized Schwarz method for elliptic problems with application to fluid-structure interaction. *Numer. Math.* **131** (2015) 369–404.
- [23] G. Gigante and C. Vergara, Optimized Schwarz method for the fluid-structure interaction with cylindrical interfaces, edited by T. Dickopf, M.J. Gander, L. Halpern, R. Krause and L.F. Pavarino. In: *Proc. of the XXII International Conference on Domain Decomposition Methods*. Springer Nature Switzerland (2016) 521–529.
- [24] J.G. Heywood, R. Rannacher and S. Turek, Artificial boundaries and flux and pressure conditions for the incompressible Navier–Stokes equations. *Int. J. Num. Methods Fluids* **22** (1996) 325–352.
- [25] C. Japhet, Optimized Krylov–Ventcell method. Application to convection-diffusion problems, edited by P.E. Bjorstad, M.S. Espedal and D.E. Keyes. In: *Proc. of the Ninth International Conference on Domain Decomposition Methods*. Springer, Berlin (1998) 382–389.
- [26] C. Japhet, N. Nataf and F. Rogier, The optimized order 2 method. Application to convection-diffusion problems. *Fut. Gen. Comput. Syst.* **18** (2001) 17–30.
- [27] N. Lebedev, *Special Functions and Their Applications*. Courier Dover Publications, Mineola, NY, USA (1972).
- [28] H. Lee, Optimal control for quasi-newtonian flows with defective boundary conditions. *Comput. Methods Appl. Mech. Eng.* **200** (2011) 2498–2506.
- [29] J.S. Leiva, P.J. Blanco and G.C. Buscaglia, Partitioned analysis for dimensionally-heterogeneous hydraulic networks. *Mult. Model. Simul.* **9** (2011) 872–903.
- [30] P.L. Lions, On the Schwarz alternating method III, edited by T. Chan, R. Glowinski, J. Periaux and O.B. Widlund, In: *Proc. of the Third International Symposium on Domain Decomposition Methods for PDE’s*. Siam, Philadelphia (1990) 202–223.
- [31] F. Magoulès, P. Ivanyi and B.H.V. Topping, Non-overlapping Schwarz method with optimized transmission conditions for the Helmholtz equation. *Comput. Methods Appl. Mech. Eng.* **193** (2004) 4797–4818.
- [32] A.C.I. Malossi, P.J. Blanco, P. Crosetto, S. Deparis and A. Quarteroni, Implicit coupling of one-dimensional and three-dimensional blood flow models with compliant vessels. *Multiscale Model Simul.* **11** (2013) 474–506.
- [33] G. Papadakis, Coupling 3d and 1d fluid–structure-interaction models for wave propagation in flexible vessels using a finite volume pressure-correction scheme. *Comm. Numer. Meth. Eng.* **25** (2009) 533–551.
- [34] A. Porpora, P. Zunino, C. Vergara and M. Piccinelli, Numerical treatment of boundary conditions to replace lateral branches in haemodynamics. *Int. J. Numer. Meth. Biomed. Eng.* **28** (2012) 1165–1183.
- [35] A. Qaddouria, L. Laayounib, S. Loiselc, J. Cotea and M.J. Gander, Optimized Schwarz methods with an overset grid for the shallow-water equations: preliminary results. *Appl. Num. Math.* **58** (2008) 459–471.
- [36] A. Quarteroni, A. Manzoni and C. Vergara, The cardiovascular system: mathematical modelling, numerical algorithms and clinical applications. *Acta Numer.* **26** (2017) 365–590.
- [37] A. Quarteroni, A. Veneziani and C. Vergara, Geometric multiscale modeling of the cardiovascular system, between theory and practice. *Comput. Methods Appl. Mech. Eng.* **302** (2016) 193–252.
- [38] B. Stupfel, Improved transmission conditions for a one-dimensional domain decomposition method applied to the solution of the Helmholtz equation. *J. Comput. Phys.* **229** (2010) 851–874.
- [39] A. Veneziani and C. Vergara, Flow rate defective boundary conditions in haemodynamics simulations. *Int. J. Num. Methods Fluids* **47** (2005) 803–816.
- [40] A. Veneziani and C. Vergara, An approximate method for solving incompressible Navier-Stokes problems with flow rate conditions. *Comput. Methods Appl. Mech. Eng.* **196** (2007) 1685–1700.
- [41] C. Vergara, Nitsche’s method for defective boundary value problems in incompressible fluid-dynamics. *J. Sci. Comput.* **46** (2011) 100–123.
- [42] I.E. Vignon-Clementel, C.A. Figueroa, K. Jansen and C. Taylor, Outflow boundary conditions for three-dimensional finite element modeling of blood flow and pressure waves in arteries. *Comput. Methods Appl. Mech. Eng.* **195** (2006) 3776–3996.
- [43] Y. Yu, H. Baek and G.E. Karniadakis, Generalized fictitious methods for fluid-structure interactions: analysis and simulations. *J. Comput. Phys.* **245** (2013) 317–346.
- [44] P. Zunino, Numerical approximation of incompressible flows with net flux defective boundary conditions by means of penalty technique. *Comput. Methods Appl. Mech. Eng.* **198** (2009) 3026–3038.